

GPU parallel computation of dendrite growth competition in forced convection using the multi-phase-field-lattice Boltzmann model

Zi-Hao Gao(高梓豪), Chang-Sheng Zhu(朱昶胜), and Cang-Long Wang(王苍龙)
Citation: Chin. Phys. B, 2023, 32 (**7**): 078101. DOI: 10.1088/1674-1056/acbc68
Journal homepage: http://cpb.iphy.ac.cn; http://iopscience.iop.org/cpb

What follows is a list of articles you may be interested in

Effect of interface anisotropy on tilted growth of eutectics: A phase field study

Mei-Rong Jiang(姜美荣), Jun-Jie Li(李俊杰), Zhi-Jun Wang(王志军), and Jin-Cheng Wang(王锦程)
Chin. Phys. B, 2022, 31 (**10**): 108101. DOI: 10.1088/1674-1056/ac76af

Amorphous transformation of ternary $Cu_{45}Zr_{45}Ag_{10}$ alloy under microgravity condition

Ming-Hua Su(苏明华), Fu-Ping Dai(代富平), and Ying Ruan(阮莹)
Chin. Phys. B, 2022, 31 (**9**): 098106. DOI: 10.1088/1674-1056/ac67c9

Numerical simulation on dendritic growth of Al-Cu alloy under convection based on the cellular automaton lattice Boltzmann method

Kang-Wei Wang(王康伟), Meng-Wu Wu(吴孟武), Bing-Hui Tian(田冰辉), and Shou-Mei Xiong(熊守美)
Chin. Phys. B, 2022, 31 (**9**): 098105. DOI: 10.1088/1674-1056/ac7211

Multi-phase field simulation of competitive grain growth for directional solidification

Chang-Sheng Zhu(朱昶胜), Zi-Hao Gao(高梓豪), Peng Lei(雷鹏), Li Feng(冯力), and Bo-Rui Zhao(赵博睿)
Chin. Phys. B, 2022, 31 (**6**): 068102. DOI: 10.1088/1674-1056/ac4486

Numerical study of growth competition between twin grains during directional solidification by using multi-phase field method

Chang-Sheng Zhu(朱昶胜), Ting Wang(汪婷), Li Feng(冯力), Peng Lei(雷鹏), and Fang-Lan Ma(马芳兰)
Chin. Phys. B, 2022, 31 (**2**): 028102. DOI: 10.1088/1674-1056/ac0eed

---

GPU parallel computation of dendrite growth competition in forced convection using the multi-phase-field-lattice Boltzmann model

Zi-Hao Gao(高梓豪)[1,3,5], Chang-Sheng Zhu(朱昶胜)[1,2,†], and Cang-Long Wang(王苍龙)[3,4,5]

[1] *College of Computer and Communication, Lanzhou University of Technology, Lanzhou* 730050, *China*
[2] *State Key Laboratory of Gansu Advanced Processing and Recycling of Non-Ferrous Metal, Lanzhou University of Technology, Lanzhou* 730050, *China*
[3] *Institute of Modern Physics, Chinese Academy of Sciences, Lanzhou* 730000, *China*
[4] *School of Nuclear Science and Technology, University of Chinese Academy of Sciences, Beijing* 100049, *China*
[5] *Advanced Energy Science and Technology Guangdong Laboratory, Huizhou* 516000, *China*

(Received 20 December 2022; revised manuscript received 28 January 2023; accepted manuscript online 16 February 2023)

A graphics-processing-unit (GPU)-parallel-based computational scheme is developed to realize the competitive growth process of converging bi-crystal in two-dimensional states in the presence of forced convection conditions by coupling a multi-phase field model and a lattice Boltzmann model. The elimination mechanism in the evolution process is analyzed for the three conformational schemes constituting converging bi-crystals under pure diffusion and forced convection conditions, respectively, expanding the research of the competitive growth of columnar dendrites under melt convection conditions. The results show that the elimination mechanism for the competitive growth of converging bi-crystals of all three configurations under pure diffusion conditions follows the conventional Walton–Chalmers model. When there is forced convection with lateral flow in the liquid phase, the anomalous elimination phenomenon of unfavorable dendrites eliminating favorable dendrites occurs in the grain boundaries. In particular, the anomalous elimination phenomenon is relatively strong in conformation 1 and conformation 2 when the orientation angle of unfavorable dendrites is small, and relatively weak in conformation 3. Moreover, the presence of convection increases the tip growth rate of both favorable and unfavorable dendrites in the grain boundary. In addition, the parallelization of the multi-phase-field-lattice Boltzmann model is achieved by designing the parallel computation of the model on the GPU platform concerning the computer-unified-device-architecture parallel technique, and the results show that the parallel computation of this model based on the GPU has absolute advantages, and the parallel acceleration is more obvious as the computation area increases.

Keywords: multi-phase field model, GPU, grain competition growth, lattice Boltzmann model

PACS: 81.30.Fb, 81.10.Aj **DOI:** 10.1088/1674-1056/acbc68

1. Introduction

Research of competitive growth between grains of different orientations is an important link in microstructures of materials. Understanding the mechanism of competitive growth of grains of different orientations, clarifying the influencing factors in the competitive growth process and then controlling the competitive growth process of grains are common and critical problems in the preparation of oriented materials.[1,2] In polycrystalline systems, the competitive growth and interaction between grains of different orientations affect the casting's final microstructure and mechanical properties, so many scholars have carry out a lot of research on the competitive growth of grains in the directional solidification process. As early as 1959, Walton and Chalmers[3] described the competitive growth process between converging dendrites of different orientations based on the analysis of the relative position of the dendrite tips and the tip sub-cooling and concluded that the dendrite tip position of unfavorably oriented dendrites has been lagging behind the dendrite tip position of favorably oriented grains and that unfavorably oriented dendrites must eliminate favorably oriented dendrites. Rappaz *et al.*[4,5] reported on this widely accepted grain competition elimination model, which graphically illustrated the elimination mechanism by studying the grain evolution organization of thin film specimens in transparent alloy experiments, and proposed the Walton–Chalmers theory. Further confirmation of the predicted results of the Walton–Chalmers model was provided by D'Souza *et al.*[6] In recent years, many scholars have identified elimination mechanisms in their research that are contrary to the Walton–Chalmers theory. Zhou *et al.*[7] observed that favorably oriented dendrites can also be eliminated by unfavorably oriented dendrites when studying the convergent bi-crystals growth during the directional solidification of the nickel-based high temperature alloy IN792. Meng *et al.*[8] found that the elimination mechanism for the competitive growth of convergent bi-crystals is the elimination of favorable dendrites by unfavorable dendrites through a combination of experiments and simulations. Li *et al.*[9] analyzed the causes of the anomalous elimination phenomenon based on physical parameters such as primary dendritic spacing and pulling speed. It can be seen that there is no systematic conclusion on the study of the competitive growth process between different morphological grains in directional solidification.

For the study of competitive grain growth in directional

[†]Corresponding author. E-mail: zhucs_2008@163.com

© 2023 Chinese Physical Society and IOP Publishing Ltd

solidification, the use of numerical simulation methods for research and analysis has become a key aspect because experimental methods cannot obtain real-time information on the tissue morphology and solute distribution during the growth evolution of dendrites. Among the many material microstructure simulation methods, the phase field method is a powerful tool developed in recent years to study the microstructure evolution process.[10] Numerous scholars have conducted more systematic studies on the process, mechanism, and control of the competitive growth of directionally solidified grains by means of phase field simulations.[11–13] In the above-mentioned studies, the elimination mechanisms in grain boundaries have been extensively described, whereas the influence of the presence of convection in grain boundaries on the evolution of bi-crystal competition has been neglected, and the dendrite morphology under pure diffusion conditions is somewhat different from the real situation when convection is present. In a recent study, Pavan *et al.*[14] used a multi-phase field model to investigate the competition for the growth of columnar dendrites under melt convection conditions. It was shown that the conventional dendrite elimination mechanism changes to an anomalous elimination growth mechanism of dendrites as the melt convection velocity gradually increases, and it was pointed out that there exists a critical melt convection velocity to determine the competitive growth mechanism at the grain boundaries. However, the study was performed only for one configuration in the competitive growth of convergent bi-crystals. To fully grasp the basic laws of polycrystalline elimination and to improve the existing theoretical model of competitive grain growth, it is necessary to consider different configurations of convergent bi-crystal systems.

The numerical solution of the phase field model has been suffered from the drawbacks of large computational effort and small computational scale. Along with the continuous updating and development of high-performance computing technology and the maturity of GPU technology in scientific computing, the CPU–GPU hybrid programming technology (CPU: central processing unit) with multi-core processor as the core is also applied to phase field simulation computation, which has gradually become one of the research frontiers in the interdisciplinary fields of computer numerical simulation and engineering, materials science, etc. In recent years, it has been confirmed in a large number of research reports[15,16] that the GPU parallel approach is fully adapted to the computation of the phase field model, which can give full play to the computational performance of GPU and effectively solve the disadvantages of computational inefficiency in the phase field model. This study developed a GPU parallel computing scheme to address these problems. By coupling the multi-phase field model and the lattice Boltzmann model (LBM), the process of competing growth of converging bi-crystals under forced convection conditions is realized. The laws of competitive growth of converging double crystals of three configurations appearing under the influence of forced convection are studied, the elimination mechanism in the evolution process is analyzed, and the problem of competitive growth of columnar dendrites under melt convection conditions is expanded.

2. Mathematical model

In this study, the multi-phase-field-lattice Boltzmann model was developed to simulate the competitive growth process of directionally solidified converging bi-crystals under forced convection. The calculation was carried out with SCN-0.24-wt% camphor model alloy (SCN: thiocyanate)[17] and developed in two-dimensional state.

2.1. Multi-phase field model

In this study, two directionally solidified grains with different orientations were simulated, and the conventional phase field model was unable to describe this orientation difference; therefore, the multi-phase field model[18] was introduced to characterize the two dendrites with different orientations. The multi-phase field model defines grains with different orientations by introducing multiple ordinal parameters φ_i $(1 <= i <= N)$ to define grains with different orientations, N is the total number of grains, and the value of φ_i varies between $[-1, 1]$, where 1 denotes the solid state and -1 denotes the liquid state, assuming that diffusion of solutes in the solid phase is not considered. For the SCN crystal with cubic symmetry, the solid-liquid interface energy anisotropy in the two-dimensional system can be expressed by

$$a(\psi) = a_{\mathrm{s}}\left(1+\frac{4\varepsilon_4}{a_{\mathrm{s}}}\right)\left[\cos^4(\theta-\Theta_{i0})+\sin^4(\theta-\Theta_{i0})\right], \quad (1)$$

where $a_{\mathrm{s}} = 1-3\varepsilon_4$, θ represents the direction of the thermal gradient and the angle perpendicular to the grain interface, ε_4 represents the anisotropic strength of the free energy at the interface, and Θ_{i0} represents the top angle of the first grain. Then, we have the multi-phase field equation

$$\begin{aligned}\tau(T)\frac{\partial\varphi_i}{\partial t} &= \nabla\cdot\left[W^2(\theta)\nabla\varphi_i\right]+\partial_x\left(|\nabla\varphi_i|^2W(\theta)\frac{\partial W^2(\theta)}{\partial(\partial_x\varphi_i)}\right)\\ &\quad+\partial_y\left(|\nabla\varphi_i|^2W(\theta)\frac{\partial W^2(\theta)}{\partial(\partial_y\varphi_i)}\right)+\varphi_i-\varphi_i^3\\ &\quad+\lambda\left(1-\varphi_i^2\right)^2\left(U+\frac{T-T_{\mathrm{ref}}}{|m|(1-k)c_l^0}\right), \quad (2)\\ \tau(T) &= \tau_0a^2(\theta-\Theta_{i0})\left[1-\frac{T-T_{\mathrm{ref}}}{|m|(1-k)c_l^0}\right], \quad (3)\end{aligned}$$

where the frozen temperature approximation $T = T_{\mathrm{ref}} + G(x-V_{\mathrm{P}}t)$ replaces the temperature, G represents the thermal gradient, T_{ref} represents the reference temperature, the pumping velocity V_{p} refers to the isotherm movement rate, x and y represent the horizontal and vertical direction axes, respectively; $c_{\mathrm{l}}^0 = c_0/k$ represents the concentration of the liquid side of the solid-liquid interface, k represents the solute partition coefficient, and c_0 represents the initial composition. The

time scale $\tau_0 = a_1 a_2 W_0^3/(d_0 D_1)$, and the space scale W_0 is determined by the solute capillary length $d_0 = a_1 W_0/\lambda$, λ denotes the width of the diffusion interface, $a_1 = 0.8839$ and $a_2 = 0.6762$;[19] $d_0 = \Gamma/\left(|m|(1-k)c_1^0\right)$, Γ represents Gibbs–Thomson coefficient, $w(\theta) = W_0 a(\theta - \Theta_{i0})$, liquidus slope $m = -1.365$ K/wt%. The dimensionless solute supersaturation U reads

$$\left[\frac{1+k}{2} - \frac{(1-k)}{2}\sum_i \varphi_i\right]\left[\frac{\partial U}{\partial t} + u\cdot\nabla U\right] = \nabla\cdot[D_1 q(\varphi)\nabla U - \boldsymbol{J}_{\rm at}] + \frac{1}{2}[1+(1-k)U] \times \sum_i \frac{\partial \varphi_i}{\partial t} - \nabla\cdot\boldsymbol{J}, \tag{4}$$

where $\boldsymbol{J}$ represents a flux associated with the fluctuation,[20] u represents the fluid velocity, $q(\varphi) = (1-\sum_i \varphi_i)/2$. $\boldsymbol{J}_{\rm at}$ represents the anti-trapping current term proposed by Karma *et al.*, [14] and the actual internal composition C of the solid and liquid phases can be determined.

$$\boldsymbol{J}_{\rm at} = -W_0[1+(1-k)U]\sum_i \partial_t \varphi_i \nabla\varphi_i/|\nabla\varphi_i|/2\sqrt{2}, \tag{5}$$

$$U = \frac{(2kc/c_\infty)/[1+k-(1-k)\sum_i \varphi_i] - 1}{1-k}. \tag{6}$$

The explicit finite difference method and the simple Euler equation are used to solve the phase field equations and the solute field equations. The grid spacing and time step are set as fixed values, with $x = 1W_0$ and $t = 0.02\tau_0$.

2.2. Lattice Boltzmann method

The lattice Boltzmann method (LBM) is utilized to compute fluid velocity, wherein the distribution function of particles in velocity and position space is represented by regular microscopic particles. These discrete particles are constrained to grid nodes, with the evolution equation establishing a discrete velocity model that yields the discrete particle distribution function. Macroscopic variables such as density and velocity are directly calculated from the particle distribution function, facilitating the calculation of the fluid's macroscopic density and velocity via the LBM. Compared to traditional numerical methods for solving Navier–Stokes equations, the LBM offers a relatively simple approach.[21]

In this study, the two-dimensional nine-velocity (D2Q9) model, depicted in Fig. 1, is employed to simulate forced convection in grain boundaries. The model's particle equilibrium state distribution function is obtained from the local particle distribution function and the continuous Boltzmann equation, which discretizes the fluid in the physical region of time and space. We present the evolution equation together with the LBM as follows:

$$f_i(r+e_i\Delta t, t+\Delta t) - f_i(r,t) = -\frac{1}{\tau_{\rm f}}\left[f_i(r,t) - f_i^{\rm eq}(r,t)\right] + \Delta t F_i(r,t), \tag{7}$$

$$f_i(r+e_i\Delta t, t+\Delta t) - f_i(r,t) = -\frac{1}{\tau_{\rm f}}\left[f_i(r,t) - f_i^{\rm eq}(r,t)\right], \tag{8}$$

$$\tau_{\rm f} = \frac{3\nu}{(c^2\Delta t)} + 0.5, \tag{9}$$

where $i = 0$–8 represents 9 directions, f_i represents the velocity distribution function of the virtual particle, $f_i^{\rm eq}$ represents the equilibrium distribution function corresponding to the virtual particle velocity, F_i represents the external force term. In the calculation of forced convection, the external source term $F_i(r,t) = 0$ due to the relatively negligible magnitude of the external force term, and the evolution equation is given in the following. Here, e_i represents the discrete velocity of the virtual particle along the direction i, r represents the spatial position vector, F_i represents the external force term, $\tau_{\rm f}$ represents the velocity relaxation time, which controls the rate of approximation of $f_i(r,t)$ to $f_i^{\rm eq}(r,t)$, and it is the time required for the particle distribution function to reach the equilibrium state from the non-equilibrium state, ν represents the kinematic viscosity of the fluid, c represents the lattice velocity, $c = \Delta x/\Delta t$, Δx represents the spatial step, and Δt represents the time step.

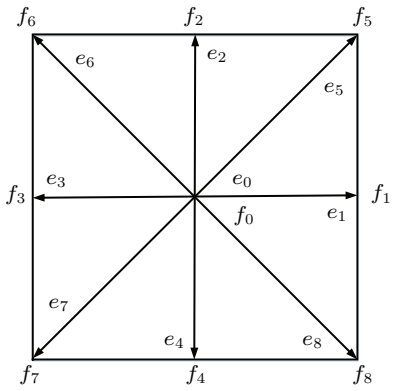


Fig. 1. Lattice structure according to D2Q9.

Also, we provide the equilibrium state distribution function as follows:

$$f_i^{\rm eq}(r,t) = \rho\omega_i\left[1 + \frac{3(e_i\cdot u)^2}{c^2} + \frac{9(e_i\cdot u)^2}{2c^2} - \frac{3u^2}{2c^2}\right], \quad i = 0,1,\ldots,8, \tag{10}$$

$$\rho = \sum f_i(r,t), \tag{11}$$

$$\rho u = \sum e_i f_i(r,t), \tag{12}$$

which includes the discrete velocity u and density ρ. Table 1 shows the values of the discrete velocity e_i and the weighting factor w_i for each particle in the model in the nine directions, respectively.

Table 1. Discrete particle velocity and weighting coefficients in the D2Q9 model.

i	0	1	2	3	4	5	6	7	8
c_x	0	c	0	$-c$	0	c	$-c$	$-c$	c
c_y	0	0	c	0	$-c$	c	c	$-c$	$-c$
w_i	4/9	1/9	1/9	1/9	1/9	1/36	1/36	1/36	1/36

2.3. Parallel method based on the CUDA technique

The multi-phase-field-lattice Boltzmann model has the biggest advantage of simulating polycrystalline systems with complex interfaces in the presence of convection. However, solving this model using traditional serial computing methods leads to low computational efficiency and time-consuming disadvantages because of the large computational volume and scale. Therefore, exploring GPU parallel computing technology has become the most effective way to solve the above problems. Figure 2 shows the schematic diagram of the computer-unified-device-architecture (CUDA) technique parallel technique used to accelerate the computation of the multi-phase-field-lattice Boltzmann model, and the overall idea of parallel design. In this design, the CPU serves as the host, which controls the start of kernel functions and the information transfer between the host and the device and runs serial code. The GPU serves as the device capable of executing multiple threads of the device in parallel. Grid, block, and thread on the device side are logically recognized to be two-dimensional. After the CPU starts the kernel, the kernel performs computational tasks on the device, creating a large number of logically two-dimensional and physically one-dimensional threads on the device, each of which can execute independently and concurrently.

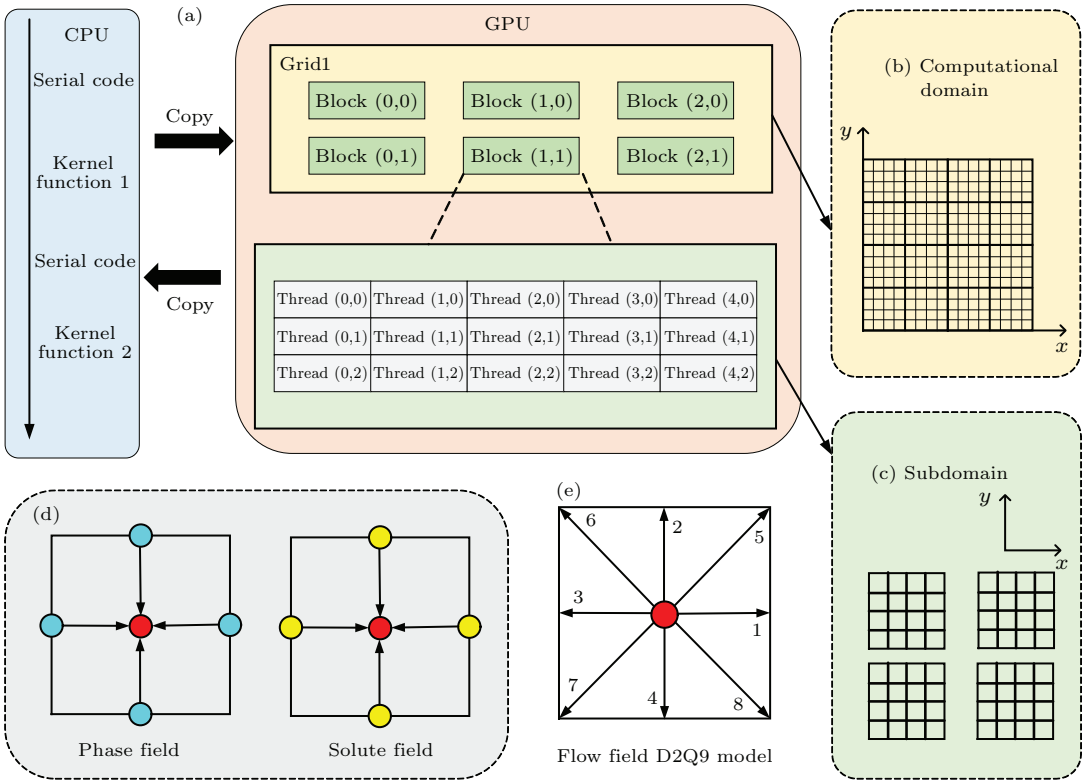


Fig. 2. Schematic diagram of the CUDA parallel accelerated multi-phase-field-lattice Boltzmann model.

As shown in Fig. 2(b), the multi-phase-field-lattice Boltzmann model divides the entire computational domain into uniform grids of the same size by the finite difference method. The LBM model constructs a grid with the same specifications as the multi-phase field model in the computational domain, and one thread is responsible for computing one grid node. When performing parallel computation on the device, the kernel function calls the grid, and all threads in the grid can cover the computation domain. As shown in Fig. 2(c), the entire computation region is divided into non-overlapping subdomains, and each corresponds to a block on the device. Stencil computation is the key to scientific computation, achieved by fixing the values of neighboring grid points on the geometric structure and calculating the update of each point in the structured grid according to the corresponding expressions. The iterative update of a large number of time steps advances the evolution of the whole computational domain system. Figure 2(d) shows the computational modes of the multi-phase field equation and solute field equation, while Fig. 2(e) shows the computational mode of the flow field equation.

The multi-phase field equation and the solute field equation both involve stencil calculations, with the former utilizing a 9-point stencil calculation and the latter a 5-point stencil calculation. Adjacent grid points on the fixed geometric structure in the computational domain have no data dependency, making the equations well-suited for parallel computation. In the D2Q9 model, the particle distribution function needs to propagate along nine directions, and an array of distribution functions must be built for each direction. As a result, the computational scale of the multi-phase-field-lattice Boltzmann model

is larger and the computational time is longer compared to the multi-phase field model. Therefore, exploring the GPU parallel method to solve the model becomes critical to improve computational efficiency.

2.4. Initial condition

In two dimensions, the meritocratic orientation of the internal dendrites of grain can be determined by the tilt angle Θ of the $\langle 100 \rangle$ direction of that grain deviating from the temperature gradient direction, where the grain deviating from the heat flow direction is the favorable grain, whose internal dendrites are the meritocratic dendrites, denoted by red, and the grain deviating from the heat flow direction is the unfavorable grain, whose internal dendrites are the meritocratic dendrites, denoted by blue. The favorable and unfavorable tilt angles are denoted by Θ_{FO} and Θ_{UO}, respectively, where clockwise deflection is assigned a negative value and counterclockwise deflection is assigned a positive value. Some of the parameters used are listed in Table 2.[17]

Table 2. Calculation parameters used in the simulation process.

Description	Parameter	Value
Kinetic viscosity	v	$1.0\times10^{-6}\ \mathrm{m^2\cdot s^{-1}}$
The solute diffusion coefficient in liquid	D_{l}	$2.7\times10^{-4}\ \mathrm{cm^2\cdot s^{-1}}$
Initial liquid temperature	T_{l}	647 °C
Gibbs–Tomson coefficient	Γ	$6.48\times10^{-6}\ \mathrm{cm\cdot K}$
Solubility partition coefficient	k	0.21
Liquidus slope	m	$-1.365\ \mathrm{K\cdot(wt.\%)^{-1}}$
The initial concentration	C_0	0.24 (wt.%)
Interface layer width parameter	ξ	54
Time discrete step size	$\mathrm{d}t$	$0.002\tau_0$

The computational domain of the initial stage is shown in Fig. 3(a), with the computational region width $W = 1500$ grids and height $H = 1500$ grids, converging bi-crystals starting from two spherical seeds, where seed F0 is a favorable grain seed with small deviation from the heat flow direction and seed U0 is an unfavorable grain seed with large deviation from the heat flow direction. After the initial stage with transient fine dendritic primary spacing, the primary spacing of the columnar dendrite in the array will evolve into a quasi-steady state. The direction of forced convection is bottom-up flow, with an initial dimensionless free flow velocity $u_{\mathrm{x}} = 0.08$. The boundary conditions are set as the periodic condition along y-direction and the no-flux condition along the x-direction (growth direction). The solid–liquid boundary of the treated flow field is in bounce format, and the external boundary is in non-equilibrium extrapolation format. To fully grasp the basic laws of polycrystalline elimination and to improve the existing theoretical model of grain competition growth, it is necessary to consider bi-crystal systems composed of grains with different orientations. For convergent bi-crystal configurations, most studies have focused on the classical convergent bi-crystal configurations by setting the orientation angle of the favorable grains to $\Theta_{\mathrm{FO}} = 0^\circ$ and setting the orientation angle of different unfavorable grains to Θ_{UO},[7–9] while there are few studies on other configurations of convergent bi-crystals. As shown in Fig. 3(b), in the multi-phase-field-lattice Boltzmann model, there are three main configurations of converging bi-crystals under forced flow, namely $\Theta_{\mathrm{FO}} \times \Theta_{\mathrm{UO}} = 0$, $\Theta_{\mathrm{FO}} \times \Theta_{\mathrm{UO}} < 0$, $\Theta_{\mathrm{FO}} \times \Theta_{\mathrm{UO}} > 0$. This paper aims to analyze the process of competing growth of different crystal orientations in converging bi-crystals under the influence of forced convection conditions, thus setting up three different signature bi-crystal orientations in each class of configurations. The three types of the configuration $\Theta_{\mathrm{FO}} \times \Theta_{\mathrm{UO}} = 0$ are A-1, A-2, and A-3; of the configuration $\Theta_{\mathrm{FO}} \times \Theta_{\mathrm{UO}} < 0$ are B-1, B-2, and B-3; of the configuration $\Theta_{\mathrm{FO}} \times \Theta_{\mathrm{UO}} > 0$ are C-1, C-2, and C-3. Table 3 lists the specific angles in the three configurations.

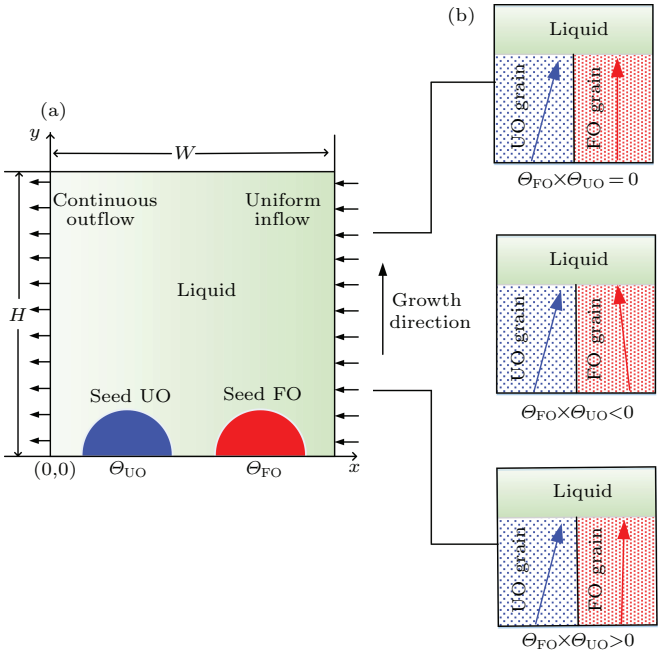


Fig. 3. (a) Condition setting of the initial state in the grain boundary, red spheres are the favorable grain seed, blue spheres are the unfavorable grain seed, and forced convection flows from the bottom-up direction. (b) Three configurations of converging bi-crystal.

Table 3. Converging configurations of bi-crystal orientations in the multi-phase-field-lattice Boltzmann model.

Case	Θ_{FO}	Θ_{UO}
A-1	0	–10
A-2	0	–15
A-3	0	–20
B-1	5	–10
B-2	5	-15
B-3	5	–20
C-1	–5	–10
C-2	–5	–15
C-3	–5	–20

3. Results and discussion

3.1. Analysis of CUDA parallel acceleration efficiency

The experimental platform is configured with Intel Core i7-9750H CPU and NVIDIA GeForce RTX 2060 GPU. For

the multi-phase-field-lattice Boltzmann model, the computational time is mainly reflected in the size of the computational domain, and the size of the computational volume depends on the number of grids. Table 4 shows the time required to compute T_C using the serial method on the CPU, and T_G using CUDA in parallel on the GPU, when other conditions are the same and the size of the computation area is different, and $t/\Delta t = 200000$. It can be seen that the advantages of GPU parallel computing will be more prominent under the same computational conditions, and the computation time is reduced substantially.

Table 4. Execution times of the CPU serial method and the GPU parallel method.

Computation area size	T_C (s)	T_G (s)
1100×1100	195827	14294
1300×1300	353243	19198
1500×1500	528210	23467

Figure 4 shows the GPU parallel computation speedup ratio to CPU serial computation as $S_N = T_C/T_G$ for all other conditions being equal and different computational domain sizes. It can be seen that there is a large difference in the acceleration effect of GPU parallel computing for different computational region sizes, as shown by the fact that the acceleration ratio of GPU parallel computing increases as the computational region increases. When the computation area size is 1500×1500, the speedup ratio is 22.5 times higher than the CPU serial program, which is 8.8 times higher than the speedup ratio when the computation area size is 1100×1100, and the speedup efficiency is significantly improved. Thus, it takes a sufficient amount of computation to bring out the computational performance of the GPU. This further demonstrates that GPU parallel solving of the multi-phase-field-lattice Boltzmann model can effectively improve the computational efficiency and scale up the computation.

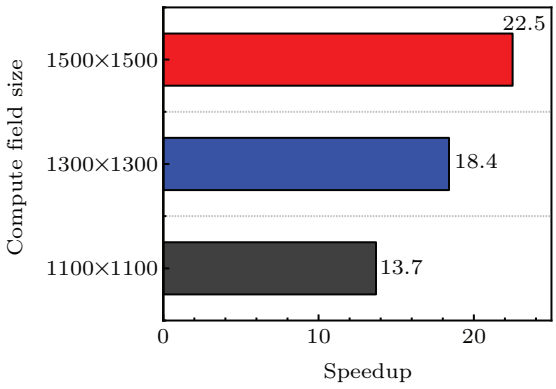


Fig. 4. GPU parallel to CPU serial acceleration ratio.

3.2. $\Theta_{FO} \times \Theta_{UO} = 0$ configuration converging bi-crystal competition growth

The classical Walton–Chalmers theory[3] suggests that during the convergent growth of bi-crystal, the favorable dendrites whose growth direction is closer to the heat flow direction will inevitably eliminate the unfavorable dendrites whose growth direction deviates significantly from the heat flow direction. However, some experiments and simulations in recent years have demonstrated[7–9] that under some specific conditions, there may be an anomalous elimination phenomenon of unfavorable dendrites eliminating the favorable dendrites. However, the elimination mechanism of converging bi-crystal of different configurations under forced convection conditions is yet to be verified.

Firstly, the competitive growth process of converging bi-crystal $\Theta_{FO} \times \Theta_{UO} = 0$ configuration was simulated under pure diffusion conditions. Figures 5(a), 5(b), and 5(c) show $\Theta_{UO} = -10°$, $\Theta_{UO} = -15°$, and $\Theta_{UO} = -20°$, respectively, converging the growth states of the dendrites, with the favorable grains in red and the unfavorable grains in blue. It can be seen that the unfavorable dendrites UO1 are all eliminated by the favorable dendrites FO1 in different grain orientations under pure diffusion conditions. Even in the subsequent evolution, the dendrite FO1 eliminates both UO2 and UO3, and this regular elimination mechanism is consistent with the Walton–Chalmers theory. In our previous research work, we focused on the analysis of the reasons for this situation. With a higher pulling velocity V_P, the favorable dendrite FO1 and the unfavorable dendrite UO1 are near each other, and UO1 is not enough to affect the growth of FO1 because the solute interaction between them is too small. And lowering the pulling speed V_P can effectively increase the solute diffusion length and enhance the solute interactions, thus making it possible for anomalous elimination to occur in the case of small Θ_{UO}.

When forced convection is applied in the grain boundary, the flow is from the bottom up and perpendicular to the direction of dendrite growth with an initial flow velocity of u_x = 0.08. Figures 5(d), 5(e), and 5(f) show the tissue morphology of converging bi-crystals with different unfavorable pickup angles under the applied flow conditions. The black arrows in the diagram indicate the direction of flow. It can be seen that when $\Theta_{UO} = -10°$, the unfavorable dendrite UO1 eliminates the favorable dendrite FO1, and the phenomenon of anomalous elimination occurs. After FO1 is blocked, the unfavorable dendrite UO1 continues to grow, and there is an obvious bending of the dendrite backbone, which is caused by the interaction between the solutes of the two dendrites. When $\Theta_{UO} = -15°$ and $\Theta_{UO} = -20°$, the elimination mechanism of converging bi-crystals is the same as that in the absence of convection, and both are the normal elimination behavior of favorable grains eliminating unfavorable grains. It is noteworthy that the unfavorable dendrite UO1 is eliminated at a smaller rate under forced convection than under pure diffusion conditions, and the convective transport mechanism near the solidification front causes some slight tilting of the FO1 dendrite arm along the flow direction, which also indicates that forced convection has an important influence on the evolutionary development of converging bi-crystal.

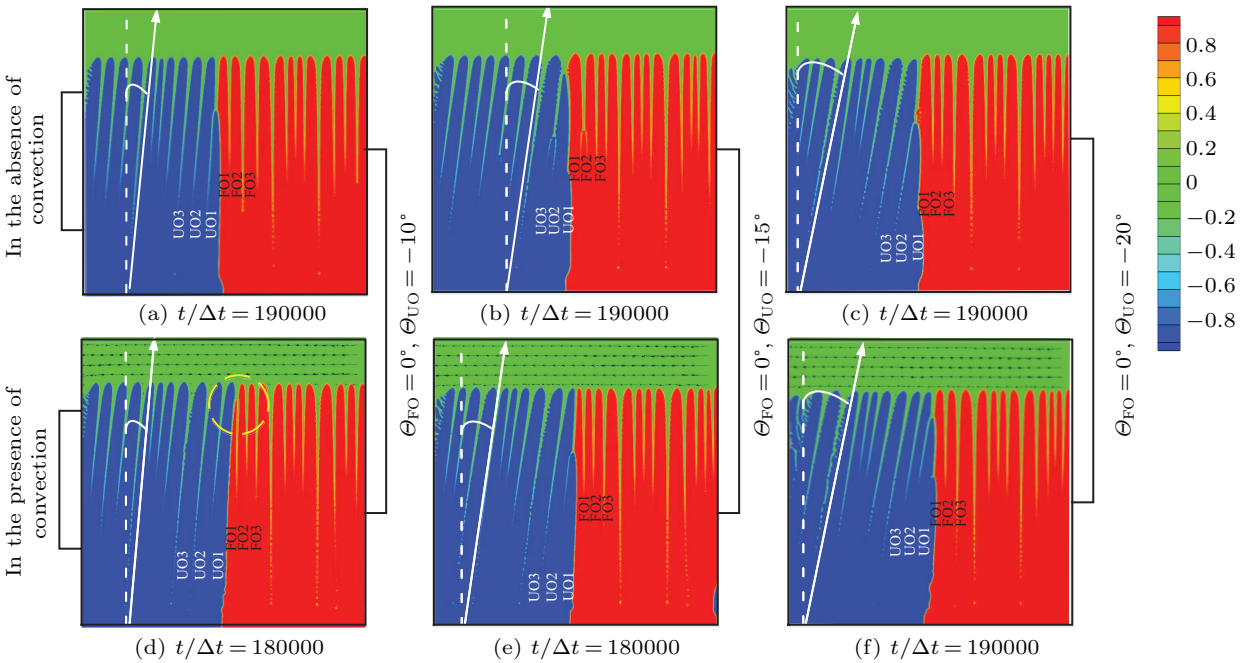


Fig. 5. Evolution results of converging bi-crystals in configuration 1 for pure diffusion condition and the presence of convection: (a) pure diffusion condition $\Theta_{UO} = -10°$, (b) pure diffusion condition $\Theta_{UO} = -15°$, (c) pure diffusion condition $\Theta_{UO} = -20°$, (d) in the presence of convection condition $\Theta_{UO} = -10°$, (e) in the presence of convection condition $\Theta_{UO} = -15°$, (f) in the presence of convection condition $\Theta_{UO} = -20°$.

To quantitatively describe the effect of forced convection on the convergent bi-crystal elimination mechanism under the same configuration and growth angle conditions, Fig. 6 shows the evolution patterns of the statistical tip height difference ΔH and primary dendrite arm spacing λ between the favorable and unfavorable grains for configuration 1, $\Theta_{UO} = -10°$, $\Theta_{UO} = -15°$ and $\Theta_{UO} = -20°$. The grain boundaries are in an unstable state at the stage of dendrite initiation growth and are stable at $t/\Delta t = 60000$, so the statistical results are analyzed from $t/\Delta t = 60000$. When $\Theta_{UO} = -10°$, the elimination mechanism of dendrites under pure diffusion conditions maintains the conventional elimination behavior of favorable grains eliminating unfavorable grains. As shown in Fig. 6(a), the tip height difference ΔH between the favorable dendrite FO1 and the favorable dendrite UO1 is greater than 0 at all evolution times (the tip of FO1 is always higher than UO1). After $t/\Delta t = 100000$, the two dendrites gradually approach the collision after which the favorable dendrite FO1 eliminates UO1. Figure 6(a1) shows the local dendrite evolution at $t/\Delta t = 120000$. The tip height difference between dendrites FO1 and UO1 is negative until $t/\Delta t = 100000$ (the tip of FO1 is always higher than that of UO1 at the beginning), but with the evolution time, the growth drive of the favorable dendrite FO1 increases and the tip height difference with the unfavorable dendrite UO2 decreases, and finally at $t/\Delta t = 120000$, the ΔH curve flattens out and the growth drive of the favorable dendrite FO1 slows down. Thereon, since the primary dendrite arm spacing λ between dendrites UO1 and FO1 is larger until $t/\Delta t = 120000$, the solute interaction between them is weak, and dendrite UO1 is not enough to affect the growth state of FO1. With the evolution of the calculation time, UO1 keeps approaching FO1, the solute interaction between the two keeps increasing, and the lateral solute cannot diffuse out, resulting in solute enrichment, which leads to a smaller growth driving force of the dendrite, thus affecting the growth of the dendrite FO1. Figure 7 shows the tip concentration curves of FO1 and UO2 at $t/\Delta t = 100000$ and $t/\Delta t = 120000$, respectively. It can be seen that as the time step increases, UO1 gets closer to FO1, the slope of the tip concentration curve of FO1 becomes slower and the solute gradient decreases accordingly, thus the growth driving force of dendrite FO1 becomes smaller, which further supports the above conclusion. After $t/\Delta t = 120000$, the tip height difference ΔH between FO1 and UO2 remains constant, and it can be speculated that the unfavorable dendrite UO2 will be eliminated in the subsequent evolution, but it is undeniable that the favorable dendrite FO1 may be eliminated in the further evolution due to the continued slowdown of the growth drive after eliminating the unfavorable dendrite several times, and the phenomenon of anomalous elimination occurs. When forced convection from the bottom up is considered, a different state occurs in the grain boundaries than previously observed, with the anomalous elimination of the unfavorable dendrite UO1 eliminating the favorable dendrite FO1. As shown in Fig. 6(b), under the influence of forced convection, the tip height difference ΔH between the favorable dendrite FO1 and the unfavorable dendrite UO1 are both negative, implying that the tip height of the dendrite UO1 is greater than that of FO1, which is due to convection scour-

ing the solute in the downstream (right) direction of the unfavorable dendrite UO1, which thins the solute layer near the tip of UO1 and thus facilitates the growth of the UO1 dendrite. Starting from $t/\Delta t = 60000$, the tip height difference between UO1 and FO1 gradually decreases until it stabilizes at $t/\Delta t = 100000$, and the tip height gradually increases after $t/\Delta t = 120000$. Therein, since the UO1 and FO1 are constantly close to each other in evolution, and the tip solutes of both interact with each other to the extent that they affect the growth drive of the dendrite until the tip height difference gradually increases after the collision of the tips of the two dendrites, implying that the unfavorable dendrite UO1 eliminates the favorable dendrite FO1. In contrast, the dendrite tips of the favorable dendrite FO2 are more driven to grow in the initial stage of the grain boundary because they are limited by flow and have no collisions with unfavorable grains. It can be observed in Fig. 6(b) that the tip of dendrite FO2 is significantly higher than that of dendrite UO1 at $t/\Delta t = 60000$, but the difference in tip height between dendrite UO1 and dendrite FO2 decreases during the subsequent evolution as the tip of UO1 increases its growth drive under the influence of forced convection. At $t/\Delta t = 120000$, the tip heights of dendrite UO1 and dendrite FO2 are the same, with the elimination of FO1, the spacing between the primary arms of UO1 and FO2 keeps decreasing, and the tip height of UO1 is significantly higher than that of FO2. When $t/\Delta t = 180000$, the local state of the dendrite is shown in Fig. 6(b2), and it can be presumed that the unfavorable dendrite UO1 will eliminate the favorable dendrite FO2 in the further evolution afterward.

When $\Theta_{\mathrm{UO}} = -15^\circ$ and $\Theta_{\mathrm{UO}} = -20^\circ$, the elimination mechanism of dendrites in both states of pure diffusion and presence of convection is the normal elimination behavior of favorable dendrites eliminating unfavorable dendrites. Assuming that the tip height difference $\Delta H = 10$ μm is the criterion for elimination of unfavorable dendrites. It can be observed from Figs. 6(a), 6(c), and 6(e) that the unfavorable dendrite UO1 with $\Theta_{\mathrm{UO}} = -20^\circ$ is eliminated at $t/\Delta t = 50000$, the unfavorable dendrite UO1 with $\Theta_{\mathrm{UO}} = -15^\circ$ is eliminated at $t/\Delta t = 90000$, and the unfavorable dendrite UO1 with $\Theta_{\mathrm{UO}} = -10^\circ$ is eliminated at $t/\Delta t = 130000$ under pure diffusion conditions. It can be seen that the size of the growth orientation angle of unfavorable dendrites is positively correlated with the elimination rate of unfavorable dendrites, implying that the larger the orientation angle, the faster the elimination rate of unfavorable dendrites. Unlike $\Theta_{\mathrm{UO}} = -10^\circ$, the tip height difference ΔH curves of the favorably oriented dendrite FO1 and the unfavorably oriented dendrite UO1 do not appear to be flat when Θ_{UO} is -15° and -20°, respectively. This is because when the orientation angle of the unfavorably oriented dendrite is larger, the two types of dendrites will have a large tip height difference due to the effect of sub-cooling, so the tip solute interaction between the two is limited when the unfavorably oriented dendrite is close to the favorably oriented dendrite. Conversely, when the orientation angle of non-favorably dendrites is small, the difference in sub-cooling between unfavorable and favorable dendrites is smaller, and the tip solutes of both dendrites interact during the approach, so the growth of the tip of favorable dendrites is limited. When convection exists in the grain boundary, due to the limited convection intensity, there is no effect on the elimination mechanism of converging bi-crystals at Θ_{UO} of -15° and -20°, respectively, and the normal elimination phenomenon of favorable dendrites eliminating unfavorable dendrites is still maintained. However, further analysis reveals that when $\Theta_{\mathrm{UO}} = -15^\circ$, the ΔH curve of dendritic FO1 and UO1 under convection condition is flatter compared to the pure diffusion state, and UO1 is eliminated at $t/\Delta t = 120000$ with a lag in elimination time compared to the pure diffusion condition. While dendrite UO2 is not eliminated during the evolution of the simulation, the ΔH curve with dendrite FO1 has been flat after $t/\Delta t = 90000$, and the tip height difference ΔH has remained positive after the elimination of dendrite UO1 (the tip height of the favorable dendrite FO1 is slightly higher than that of the unfavorable dendrite UO1), but the curve trend has a slight decrease. It can be seen that the current elimination mechanism of convection on grain boundaries has not changed, but the influence on the growth evolution of dendrites in grain boundaries has been present. We measured the tip height difference between dendrite FO1 and dendrite UO3 at $t/\Delta t = 190000$ for the pure diffusion condition and $t/\Delta t = 180000$ for the condition with convection, respectively. It can be seen that the tip height of UO3 in the pure diffusion condition is much lower than that of dendrite FO1, while the tip height difference ΔH is negative in the presence of convection, implying that the tip height of UO3 is higher than that of dendrite FO1. It can be speculated that the dendrite UO3 under pure diffusion conditions will still be eliminated, and the presence of convection in the grain boundary will continue to affect the growth of dendrites, which may change the original dendrite elimination mechanism during subsequent evolution, implying that there is a probability that the unfavorable UO3 will eliminate the favorable dendrite FO1. Unlike the other two unfavorable orientation angles, $\Theta_{\mathrm{UO}} = -20^\circ$, although the elimination times of dendrites UO1 and UO2 are larger than those under pure diffusion conditions, the tip height of dendrite UO3 is still much smaller than that of dendrite FO1 in the simulated time due to the excessive unfavorable pickup angle. It can be inferred that forced convection has limited ability to affect dendrite growth under these conditions, and the elimination mechanism in the grain boundary will continue to be the elimination of unfavorable dendrites by favorable dendrites.

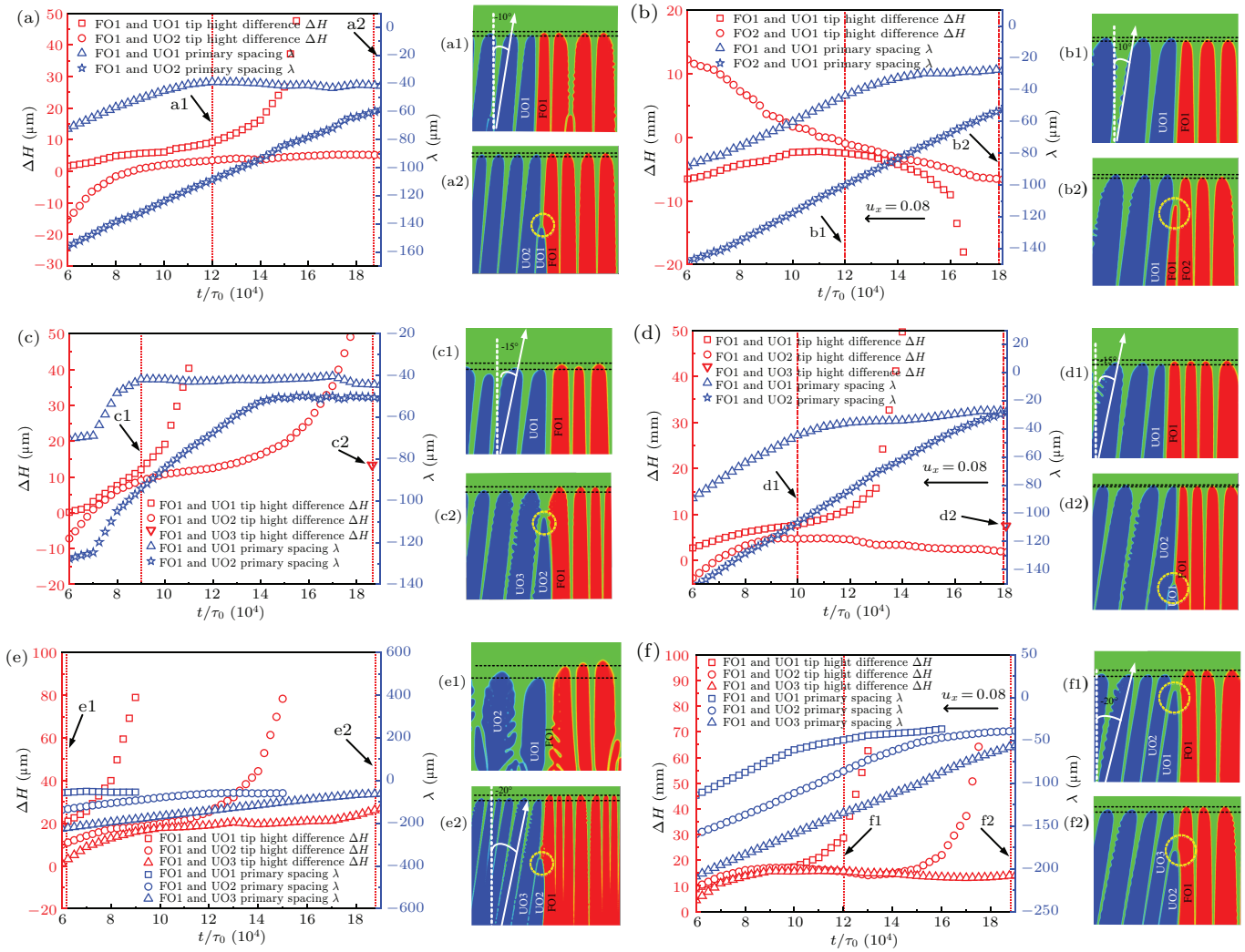


Fig. 6. Evolution of the primary arm spacing λ and tip height difference ΔH between favorable and unfavorable dendrites for pure diffusion and presence of convection in configuration 1: (a) pure diffusion condition $\Theta_{UO} = -10°$, (b) in the presence of convection condition $\Theta_{UO} = -10°$, (c) pure diffusion condition $\Theta_{UO} = -15°$, (d) in the presence of convection condition $\Theta_{UO} = -15°$, (e) pure diffusion condition $\Theta_{UO} = -20°$, (f) in the presence of convection condition $\Theta_{UO} = -20°$.

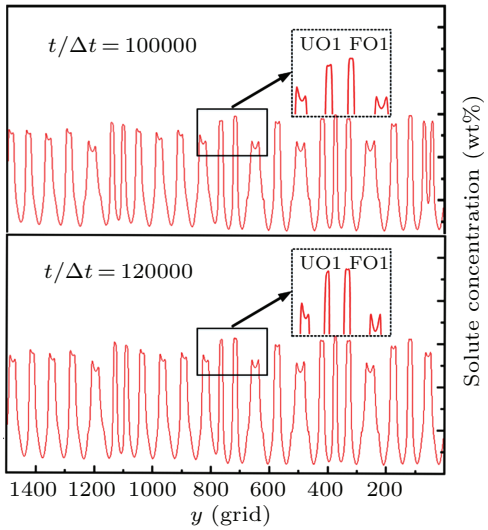


Fig. 7. Tip concentration profiles of FO1 and UO2 at $t/\Delta t = 100000$ and $t/\Delta t = 120000$.

The dendrite tip height at time step T is H_T, the time step interval is ΔT, and the growth rate of the dendrite tip is $S = (H_T - H_{T-1})/(\Delta T)$. Figures 8(a)–8(c) show the tip growth rate of favorable and unfavorable dendrites in each time step under pure diffusion and presence of convection for $\Theta_{UO} = -10°$, $\Theta_{UO} = -15°$, and $\Theta_{UO} = -20°$, respectively. It can be seen that the highest dendrite tip growth rate is observed at $t/\Delta t = 70000$ for all dendrites under pure diffusion conditions and shows a decreasing trend until the rate levels off. This is due to the low enrichment of solutes at the dendrite tips during the initial stage of dendrite growth and the large growth rate of dendrites. With further evolution, the solute gradually accumulates at the dendrite tip, leading to a slowdown in the growth rate of the dendrite tip until the tip growth rate tends to level off when the solute is uniformly distributed throughout the calculated region. In contrast, when convection is present in the grain boundary, it can be seen that there is a transient increase in the dendrite tip growth rate at the beginning, and the tip rate is inversely proportional to the fetch angle of the unfavorable dendrite, implying that the larger the fetch angle of the unfavorable dendrite, the smaller the increase in the dendrite tip rate. In contrast, when convection is present in the grain

boundary, it can be seen that there is a transient increase in the dendrite tip growth rate at the beginning, and the tip rate is inversely proportional to the fetch angle of the unfavorable dendrite, implying that the larger the fetch angle of the unfavorable dendrite, the smaller the increase in the dendrite tip rate. The average tip growth rate of dendrites in the presence of convection is set to $\bar{S}_c$, the average tip growth rate of dendrites in pure diffusion is $\bar{S}$, and the difference between the average tip growth rates of the two states is $\Delta S = \bar{S}_c - \bar{S}$.

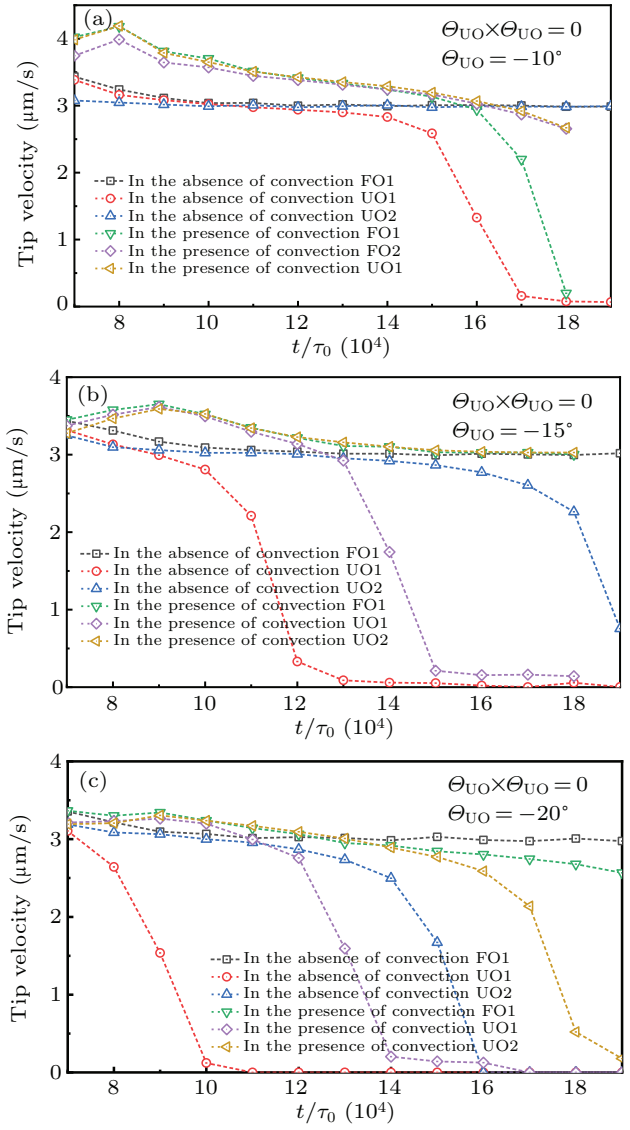


Fig. 8. Tip growth rates of favorable and unfavorable dendrites in configuration 1 with pure diffusion and in the presence of convection: (a) $\Theta_{UO} = -10°$, (b) $\Theta_{UO} = -15°$, (c) $\Theta_{UO} = -20°$.

Figure 9 shows the average tip growth rates of favorably oriented dendrite FO1 and unfavorably oriented dendrite UO1 for $\Theta_{UO} = -10°$, $\Theta_{UO} = -15°$, and $\Theta_{UO} = -20°$, as well as the difference in the average tip growth rates of FO1 and UO1 under pure diffusion and convection conditions. When $\Theta_{UO} = -10°$, the average tip velocity differences between FO1 and UO1 under convection and pure diffusion conditions, respectively: $\Delta S_{FO1} = 0.34$ μm/s, $\Delta S_{UO1} = 0.59$ μm/s. When $\Theta_{UO} = -15°$, the average tip velocity differences of dendrites FO1 and UO1 under convection and pure diffusion conditions, respectively: $\Delta S_{FO1} = 0.17$ μm/s, $\Delta S_{UO1} = 0.51$ μm/s. When $\Theta_{UO} = -20°$, the average tip velocity differences of dendrites FO1 and UO1 under convection and pure diffusion conditions, respectively: $\Delta S_{FO1} = -0.06$ μm/s, $\Delta S_{UO1} = 0.46$ μm/s. It can be seen that the presence of convection in the grain boundary has a significantly greater effect on the growth rate of unfavorable dendrite tips than on the growth rate of favorable dendrite tips. With the gradual increase of the orientation angle of the unfavorable dendrites, the average tip velocity difference between FO1 and UO1 in the convective and pure diffusion conditions shows a gradient decrease, which means that the influence of the presence of convection in the grain boundary on the growth rate of both dendrites decreases with the increase of Θ_{UO}. Further analysis reveals that when the orientation angle Θ_{UO} of unfavorable dendrites is small, the overall growth rate of dendrites with convection in the grain boundary is larger than that of dendrites with pure diffusion, and when $\Theta_{UO} = -20°$, the tip growth rate of FO1 of favorable dendrites under convection conditions will slightly lag behind that of FO1 with pure diffusion. Under convective conditions, the tip growth rate of unfavorable dendrite UO1 slows down with the increase of the orientation angle of unfavorable dendrite but is always greater than the tip growth rate in the pure diffusion state, which is due to the continuous scouring of the solute in the downstream (right) direction of the dendrite UO1 by the flow and the thinning of the solute layer near the tip of UO1, so that the tip growth rate of UO1 is always greater than the pure diffusion state.

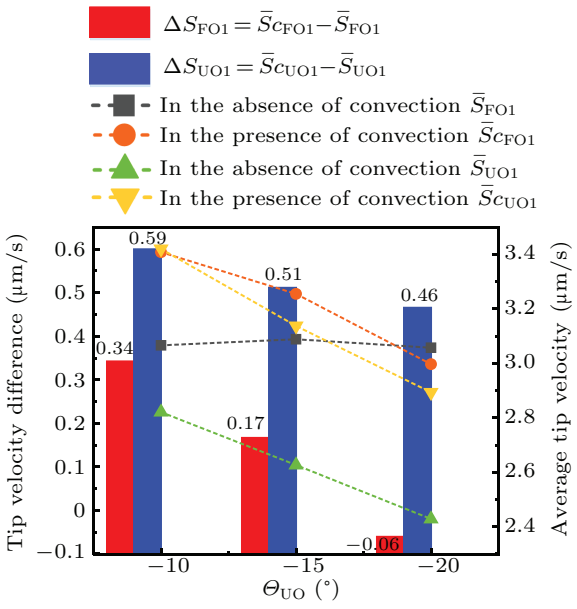


Fig. 9. Average tip growth rates for $\Theta_{UO} = -10°$, $\Theta_{UO} = -15°$, and $\Theta_{UO} = -20°$ in configuration 1 for the favorably oriented dendrite FO1 and the unfavorably oriented dendrite UO1, and the average tip growth rate difference between FO1 and UO1 in the two states.

In summary, convection can effectively increase the growth rate of unfavorable dendrites at grain boundaries dur-

ing the evolution of converging bi-crystals of configuration 1, and this effect decreases with the increase of the orientation angle of unfavorable dendrites. As for the favorable dendrites, when Θ_{UO} is small, the tip growth rate of favorable dendrites under convection conditions is larger, and when Θ_{UO} is large, convection has no significant effect on increasing the tip growth rate of favorable dendrites.

3.3. $\Theta_{FO} \times \Theta_{UO} < 0$ configuration converging bi-crystal competition growth

Figure 10 shows the competitive growth process of converging bi-crystals of $\Theta_{FO} \times \Theta_{UO} < 0$ configuration under pure diffusion conditions and in the presence of convection, respectively. The right side is the dendrites of the favorable grains (red) and the angle taken by the favorable grains is $\Theta_{FO} = 5°$. The left side is the dendrites of the unfavorable grains (blue), and the unfavorable grains take the angles $\Theta_{UO} = -10°$, $\Theta_{UO} = -15°$, and $\Theta_{UO} = -20°$, respectively. At this point, the two grains of convergent growth are tilted in opposite directions. Under the pure diffusion condition, the elimination mechanism of converging bi-crystals with three different angle combinations in configuration 2 remains the same as that in configuration 1, which are all normal elimination behaviors of favorable grains eliminating unfavorable grains. As the orientation angle of the unfavorable grains increases, the more favorable dendrites eliminate the unfavorable dendrites. When convection conditions exist in the grain boundary, $\Theta_{UO} = -10°$, the unfavorable dendrites block out the favorable dendrites in the process of approaching the favorable dendrites, and anomalous elimination occurs. When $\Theta_{UO} = -15°$ and $\Theta_{UO} = -20°$, both the favorable dendrites eliminate the unfavorable dendrites.

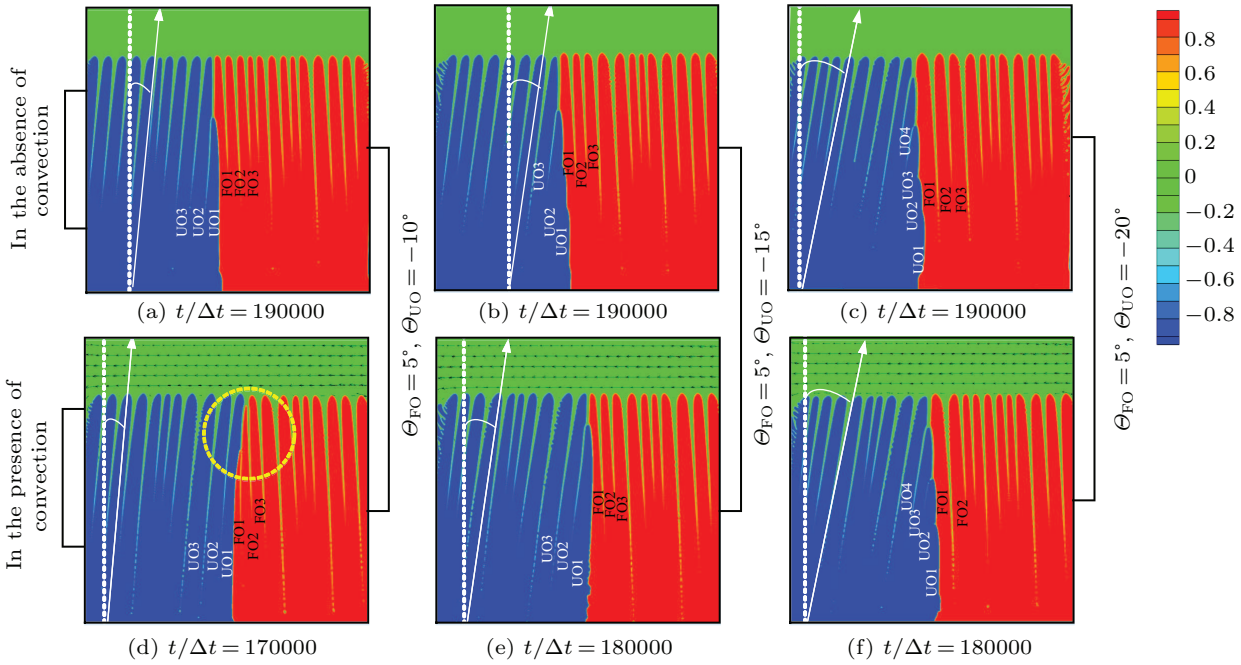


Fig. 10. Evolution results of converging bi-crystals in configuration 2 for pure diffusion condition and the presence of convection: (a) pure diffusion condition $\Theta_{UO} = -10°$, (b) pure diffusion condition $\Theta_{UO} = -15°$, (c) pure diffusion condition $\Theta_{UO} = -20°$, (d) in the presence of convection condition $\Theta_{UO} = -10°$, (e) in the presence of convection condition $\Theta_{UO} = -15°$, (f) in the presence of convection condition $\Theta_{UO} = -20°$.

Figure 11 shows the evolution pattern of the statistical tip height difference ΔH and primary dendrite arm spacing λ between the favorable and unfavorable grains with the calculated time step for configuration 2, $\Theta_{UO} = -10°$, $\Theta_{UO} = -15°$, and $\Theta_{UO} = -20°$. When $\Theta_{UO} = -10°$, the elimination mechanism of dendrites under pure diffusion conditions maintains the conventional elimination behavior of favorable grains eliminating unfavorable grains. Compared with configuration 1, the difference between the tip heights of FO1 and UO1 in configuration 2 in the starting state is smaller, thus the solute interaction between the tips of FO1 and UO1 is stronger, and the elimination time of UO1 is slightly lagged compared to that in configuration 1. In the convective state, FO1 is eliminated faster in configuration 2 compared with configuration 1. In the process of elimination, the tip height difference curves of FO2 and UO1 show a flattening, and FO2 is also eliminated successively at $t/\Delta t = 150000$. It is worth noting that the unfavorable dendrite UO1 eliminates both the favorable dendrites FO1 and FO2 for $t/\Delta t = 170000$ in configuration 2, while only FO1 is eliminated for $t/\Delta t = 180000$ in configuration 1. At $\Theta_{UO} = -15°$, unlike in configuration 1, the number of unfavorable dendrites is eliminated more during the evolution of the pure diffusion condition. In the presence of convection, the unfavorable dendrites are eliminated with a more delayed

time compared to configuration 1. During the elimination of dendrite UO1, the tip height difference curve between UO2 and FO1 decreases, and ΔH tends to 0 at $t/\Delta t = 180000$, but ΔH keeps a positive value, implying that the tip height of the favorable dendrite FO1 is slightly higher than that of the unfavorable dendrite UO1, and the elimination mechanism is still normal elimination. However, at $t/\Delta t = 180000$, the difference in tip height between FO1 and UO3 was measured in the presence of convective conditions in the dendrite, and ΔH was negative, implying that the tip height of UO3 is higher than that of FO1. It can be inferred that the unfavorable dendrite UO3 may eliminate the dendrite FO1 in the subsequent evolution, which is consistent with the pattern in configuration 1. When $\Theta_{UO} = -20°$, the number of unfavorable dendrites eliminated is higher in both the convective and pure diffusion states for configuration 2 compared to configuration 1. It is worth noting that in the initial state ($t/\Delta t = 160000$), the tip height of the unfavorable dendrite in configuration 2 is essentially the same as that of the favorable dendrite, and even the tip height of the unfavorable dendrite is higher than that of the favorable dendrite under pure diffusion conditions.

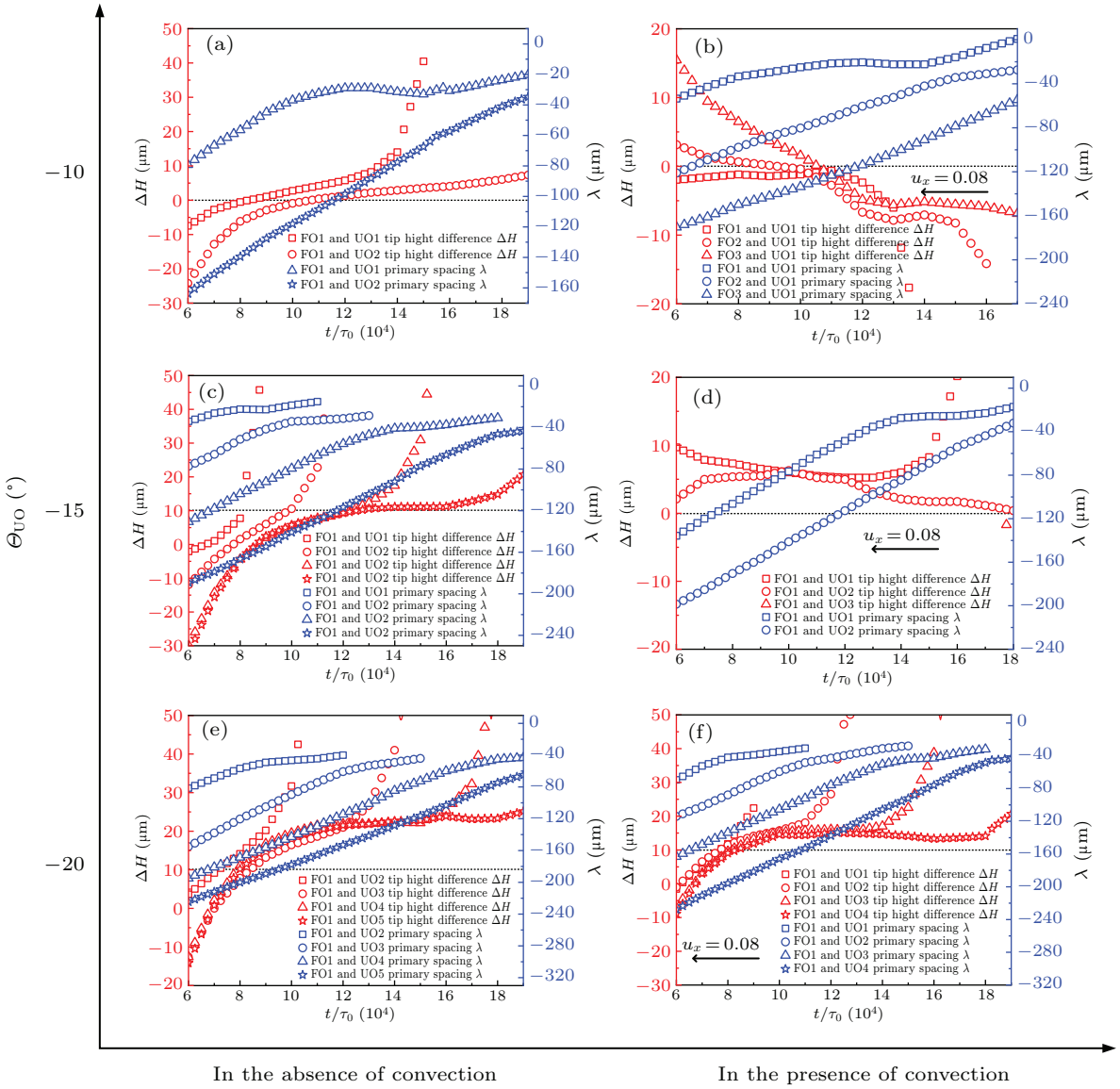


Fig. 11. Primary arm spacing λ and tip height difference ΔH between favorable and unfavorable dendrites for pure diffusion and presence of convection in configuration 2: (a) pure diffusion condition $\Theta_{UO} = -10°$, (b) in the presence of convection condition $\Theta_{UO} = -10°$, (c) pure diffusion condition $\Theta_{UO} = -15°$, (d) in the presence of convection condition $\Theta_{UO} = -15°$, (e) pure diffusion condition $\Theta_{UO} = -20°$, (f) in the presence of convection condition $\Theta_{UO} = -20°$.

To further analyze the evolution pattern of dendrites in configuration 2, consistent with the setup in the above section, Figure 12 shows the tip growth rates of favorable and unfavorable dendrites for $\Theta_{UO} = -10°$, $\Theta_{UO} = -15°$, and $\Theta_{UO} = -20°$ in the presence of convection and pure diffusion conditions. It can be seen that under pure diffusion conditions, the tip growth rate of all dendrites shows a decreasing trend until it levels off when the solute distribution in the grain boundaries is uniform. When convection is present in the grain boundary, all dendrite tip rates show a decreasing trend after a short increase. With

the increase of the orientation angle of the unfavorable dendrite, the increase of the dendrite tip growth rate in the initial stage becomes smaller, and the above evolution pattern is consistent with that of configuration 1. Unlike in configuration 1, the tip growth rate of the dendrite in configuration 2 under convection conditions is essentially the same as the tip growth rate in the presence of pure diffusion in the initial stage ($t/\Delta t = 70000$). Even at $\Theta_{UO} = -15°$, the tip growth rate of FO1 under pure diffusion conditions is larger than that in the presence of convection in the initial stage.

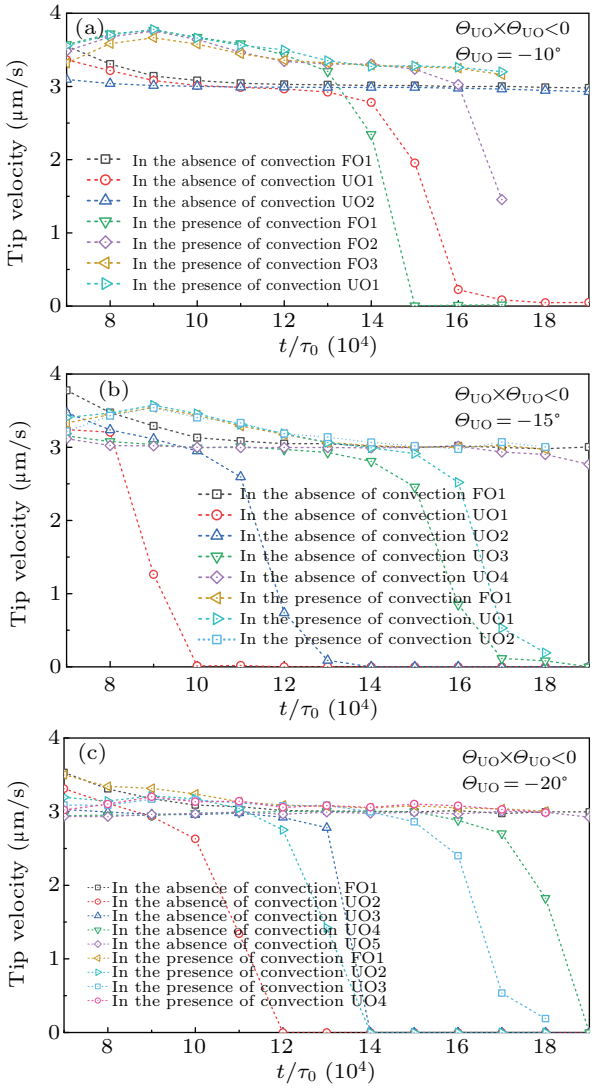


Fig. 12. Tip growth rates of favorable and unfavorable dendrites in configuration 2 with pure diffusion and the presence of convection: (a) $\Theta_{UO} = -10°$, (b) $\Theta_{UO} = -15°$, (c) $\Theta_{UO} = -20°$.

Figure 13 shows the average tip growth rates of the favorably oriented dendrite FO1 and the unfavorably oriented dendrite UO1 for the unfavorably oriented dendrite taking angles of $\Theta_{UO} = -10°$, $\Theta_{UO} = -15°$, and $\Theta_{UO} = -20°$ in configuration 2, and the average tip growth rate difference between FO1 and UO1 in the two states. When $\Theta_{UO} = -10°$, the average tip velocity differences between FO1 and UO1 under convection and pure diffusion conditions are $\Delta S_{FO1} = 0.32$ μm/s, $\Delta S_{UO1} = 0.54$ μm/s. When $\Theta_{UO} = -15°$, the average tip velocity differences of dendrites FO1 and UO1 under convection and pure diffusion conditions are $\Delta S_{FO1} = 0.05$ μm/s, $\Delta S_{UO1} = 0.48$ μm/s. When $\Theta_{UO} = -20°$, the average tip velocity differences of dendrites FO1 and UO1 under convection and pure diffusion conditions are $\Delta S_{FO1} = 0.07$ μm/s, $\Delta S_{UO1} = 0.18$ μm/s. It can be seen that, in agreement with configuration 1, the presence of convection in the grain boundary also has a significantly greater effect on the growth rate of unfavorable dendrite tips than that on the growth rate of favorable dendrite tips. Unlike configuration 1, ΔS_{FO1} and ΔS_{UO1} in configuration 2 always maintain positive values. It can be seen that for any value of Θ_{UO}, the tip growth rate of the dendrite in the presence of convection is larger than that of the dendrite under the pure diffusion condition, and the average tip velocity difference between the unfavorable dendrite UO1 in the convection and pure diffusion conditions decreases in a gradient manner, while the tip velocity difference of the favorable dendrite FO1 does not decrease at $\Theta_{UO} = -15°$ and $\Theta_{UO} = -20°$. It is worth noting that (1) the growth rates of dendrite tips in FO1 and UO1 in configuration 2 are greater than the tip growth rates of dendrites in configuration 1 in the presence of both convection and pure diffusion. (2) The average tip velocity differences ΔS_{FO1} and ΔS_{UO1} for FO1 and UO1 in configuration 2 under convective and pure diffusion conditions, respectively, are smaller overall than those of configuration 1. It is known that convection in the grain boundary has less influence on the convergent bi-crystal growth in configuration 2 than in configuration 1.

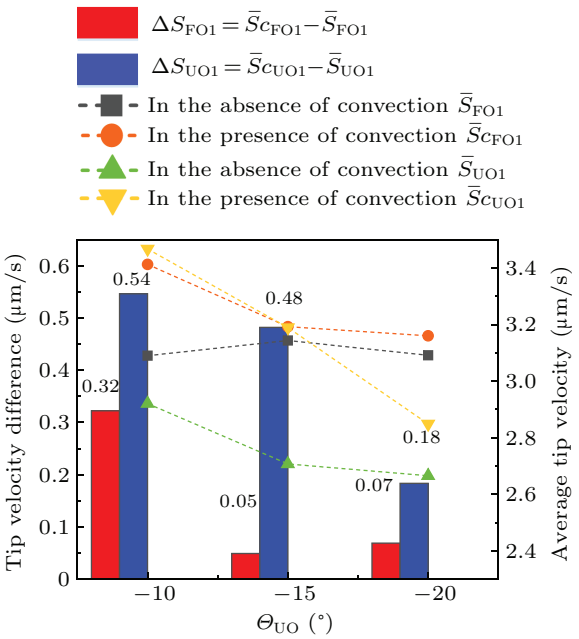


Fig. 13. Average tip growth rates for $\Theta_{UO} = -10°$, $\Theta_{UO} = -15°$, and $\Theta_{UO} = -20°$ in configuration 2 for the favorably oriented dendrite FO1 and the unfavorably oriented dendrite UO1, and the average tip growth rate difference between FO1 and UO1 in the two states.

3.4. $\Theta_{FO} \times \Theta_{UO} > 0$ configuration converging bi-crystal competition growth

Figure 14 shows the competitive growth process of converging bi-crystals of $\Theta_{FO} \times \Theta_{UO} > 0$ configuration under pure diffusion conditions and in the presence of convection, respectively. The right side is the dendrites of the favorable grains (red) and the angle taken by the unfavorable grains is $\Theta_{FO} = -5°$. The left side is the dendrites of the unfavorable grains (blue), and the unfavorable grains take the angles $\Theta_{UO} = -10°$, $\Theta_{UO} = -15°$, and $\Theta_{UO} = -20°$. At this time, the tilt direction of the two grains growing together is the same. It can be seen that, under pure diffusion conditions, the normal elimination phenomenon of favorable dendrites eliminating unfavorable dendrites at convergent grain boundaries is evident for both Θ_{UO} of $-15°$ and $-20°$ in configuration 3. However, for $\Theta_{UO} = -10°$, there is already a clear trend of normal elimination, but the unfavorable dendrites have not been completely eliminated during the evolution time, and the grain boundaries are along the growth direction of the favorable dendrites. Similar to the above two configurations, configuration 3 also under pure diffusion conditions, as the orientation angle of the unfavorable grains increases, the more the favorable dendrites eliminate the unfavorable dendrites. When convection is present in the grain boundary, the unfavorable dendrite UO1 with $\Theta_{UO} = -10°$ shows a tendency to eliminate the favorable dendrite FO1. In the other two angles, the elimination is normal, but the elimination time lags and the number of eliminated dendrites is smaller compared to the pure diffusion condition.

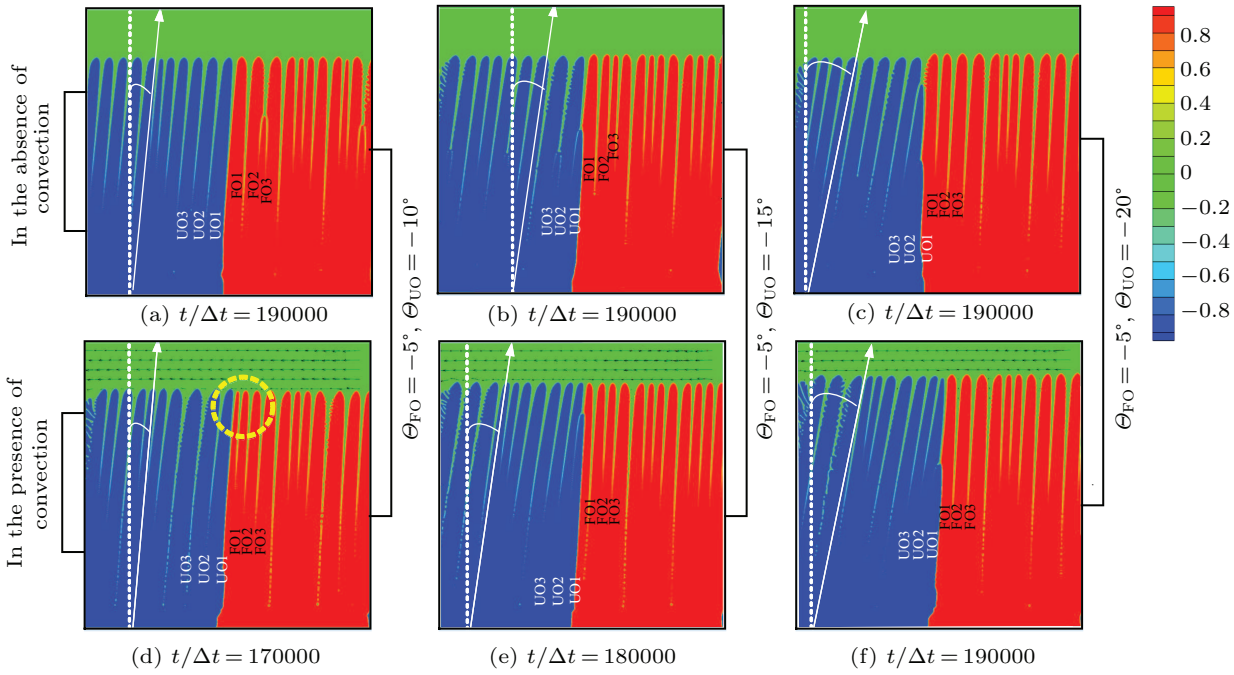


Fig. 14. Evolution results of converging bi-crystals in configuration 3 under pure diffusion condition and in the presence of convection: (a) under pure diffusion condition $\Theta_{UO} = -10°$, (b) under pure diffusion condition $\Theta_{UO} = -15°$, (c) under pure diffusion condition $\Theta_{UO} = -20°$, (d) in the presence of convection condition $\Theta_{UO} = -10°$, (e) in the presence of convection condition $\Theta_{UO} = -15°$, (f) in the presence of convection condition $\Theta_{UO} = -20°$.

The tip height difference ΔH and the primary dendrite arm spacing λ, between the favorable and unfavorable grains of the three angles in configuration 3, were accounted for the evolution with time. As shown in Fig. 15, when $\Theta_{UO} = -10°$, the tip height difference between the favorable and unfavorable dendrites under the pure diffusion condition keeps increasing trend and is positive after the evolution time $t/\Delta t = 90000$, which shows that the elimination mechanism is still the elimination of unfavorable dendrites by the favorable dendrites. When convective conditions exist, the overall evolution pattern is just the opposite of the pure diffusion state, and the tip height difference between the favorable and unfavorable dendrites tends to increase during the evolution time, and the elimination mechanism is changed and anomalous elimination occurs. When $\Theta_{UO} = -15°$, the tip height difference between the favorable and unfavorable dendrites in the pure diffusion state remains positive from the beginning and shows an increasing trend, in agreement with the other two configurations. During the elimination of UO1, the growth rate of dendrite FO1 is affected, thus the tip height difference curve with UO1 tends to level off until it starts to increase after $t/\Delta t = 170000$. In contrast, the influence of flow on the growth rate of unfavorable dendrites in the convective state leads to a negative tip height difference between the favorable and unfavorable dendrites in the beginning stage, and the elimination time of unfavorable dendrites is relatively lagged. After

$t/\Delta t = 120000$, the tip height difference curves of dendrites UO2 and FO1 show a decreasing trend, and ΔH is negative when $t/\Delta t = 180000$. It can be predicted that the favorable dendrite FO1 may be eliminated in the subsequent evolution, and the elimination mechanism may switch from normal elimination to anomalous elimination. It is worth noting that when $\Theta_{UO} = -15°$, the tip height difference between the unfavorable dendrites and FO1 is negative at the final evolution time for the three configurations counted in the paper. Conformations 1 and 2 are the ones where the tip height difference between UO3 and FO1 is negative after the elimination of UO1 and UO2, while conformation 3 is the one where the tip height difference between UO2 and FO1 is negative after the elimination of UO1.

It can be seen that the elimination mechanism may change from normal to anomalous elimination under the continuous influence of convection for the three configurations at $\Theta_{UO} = -15°$. When $\Theta_{UO} = -20°$, consistent with the other two configurations, convection has a limited effect on the competitive growth of dendrites and does not affect the original elimination mechanism, except for a slowdown in the elimination time of unfavorable dendrites. However, compared with the other two conformations, the number of unfavorable dendrites eliminated in the evolution time of conformation 3 is smaller than that of the other two conformations. In summary, under arbitrary state conditions, the number of eliminated dendrites in configuration 3 is less than the other two configurations due to the smaller differentiation of the two dendrite pickup angles in configuration 3 compared to configurations 1 and 2, regardless of whether the elimination mechanism in the grain boundary is normal or anomalous elimination.

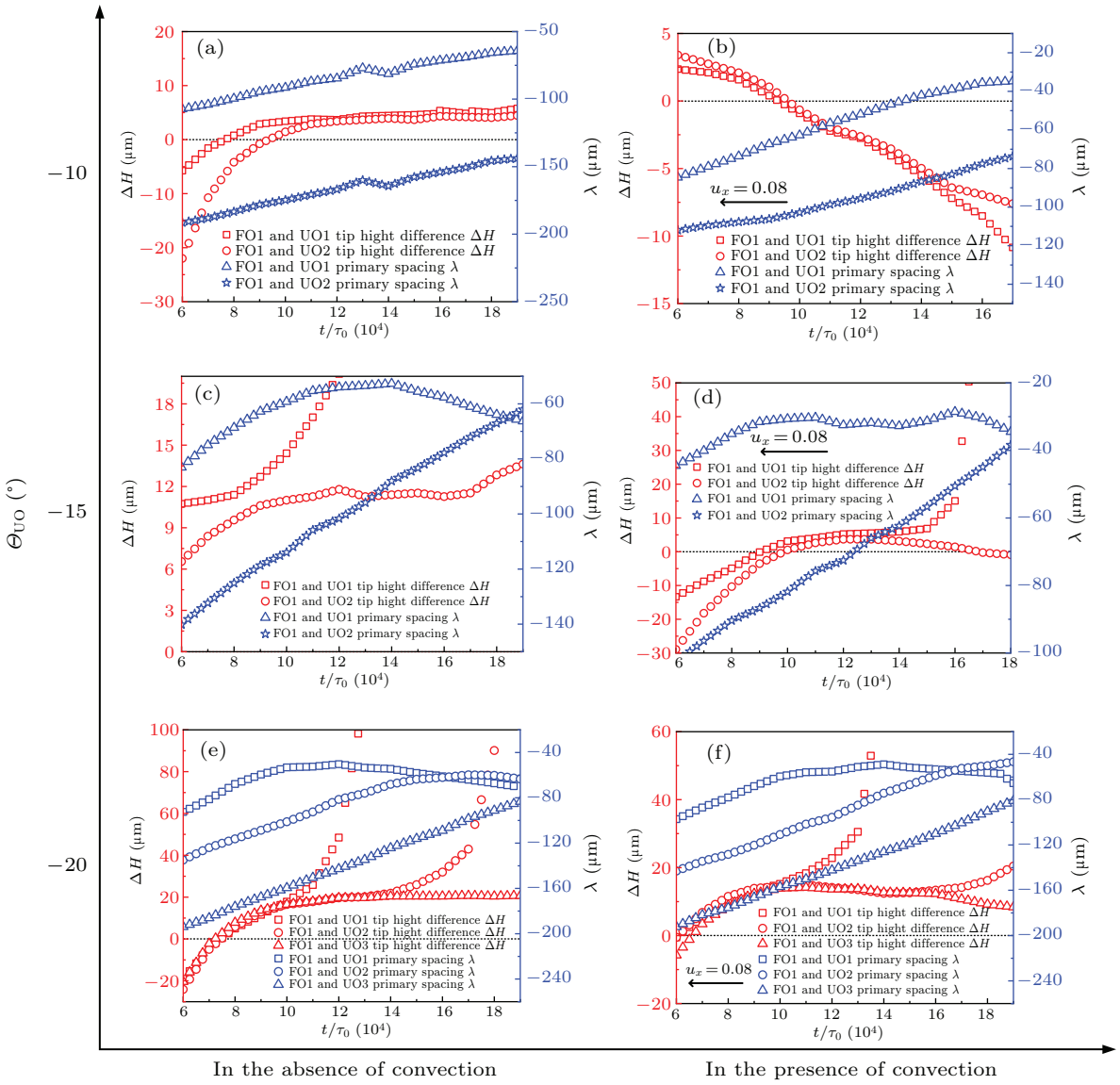


Fig. 15. Primary arm spacing λ and tip height difference ΔH between favorable and unfavorable dendrites for pure diffusion and in presence of convection in configuration 3: (a) under the pure diffusion condition $\Theta_{UO} = -10°$, (b) in the presence of convection condition $\Theta_{UO} = -10°$, (c) under the pure diffusion condition $\Theta_{UO} = -15°$, (d) in the presence of convection condition $\Theta_{UO} = -15°$, (e) under the pure diffusion condition $\Theta_{UO} = -20°$, (f) in the presence of convection condition $\Theta_{UO} = -20°$.

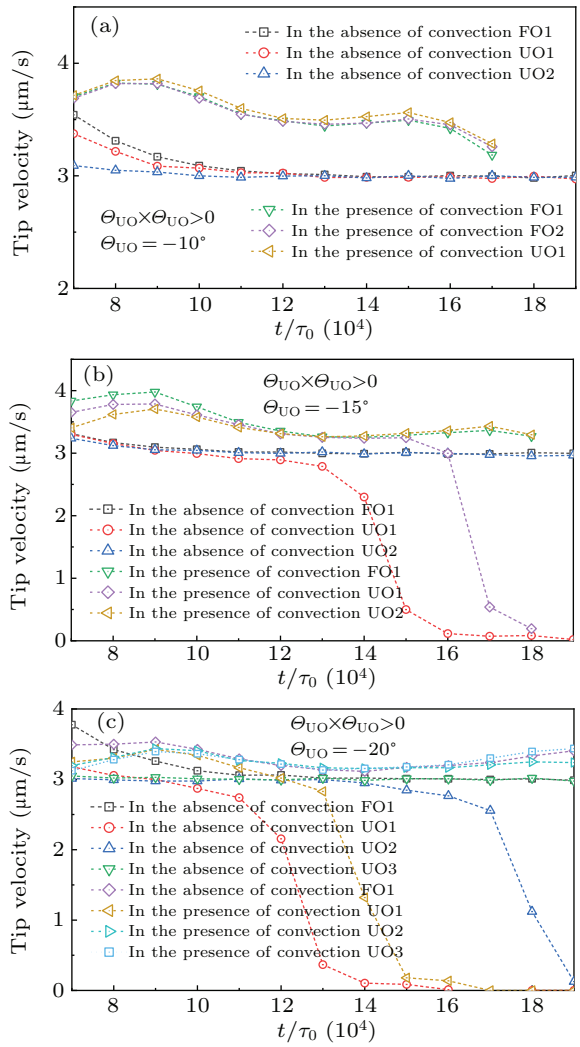


Fig. 16. Tip growth rates of favorable and unfavorable dendrites in configuration 3 with pure diffusion and in the presence of convection: (a) $\Theta_{UO}=-10°$, (b) $\Theta_{UO}=-15°$, (c) $\Theta_{UO}=-20°$.

Figure 16 shows the tip growth rates of the three angles in configuration 3 under convective and pure diffusion conditions for both favorable and unfavorable dendrites during the evolution time. It can be seen that under pure diffusion conditions, the growth rate of the dendrite tip evolves with time in a pattern consistent with those of conformation 1 and conformation 2, both growth rates for favorable and unfavorable dendrites decrease monotonically with the evolution of the time step. When convection is present in the grain boundary, it can be seen that the tip growth rate of all dendrites increases and then decreases at the beginning, and then increases again to a certain value and then decreases, showing an overall wavy curve, which is significantly different from the other two configurations. It is worth noting that in the convective state, $\Theta_{UO}=-10°$, the tip rates of the favorable and unfavorable dendrites in the starting phase remain basically the same, and when the orientation angle of the unfavorable dendrites increases ($\Theta_{UO}=-15°$, $\Theta_{UO}=-20°$), the tip growth rate of the favorable dendrites is significantly larger than that of the unfavorable dendrites for some time starting from $t/\Delta t=70000$. After that, under the continuous influence of convection, the tip growth rate of unfavorable dendrites gradually increases, and the difference in tip growth rate between the two dendrites then decreases. In analysis, it was found that the tilt direction of the favorable and unfavorable grains is the same in configuration 3, while the direction of the flow with forced convection imposed in the grain boundaries is flowing from the bottom up. Therefore, the flow scours the downstream (right) direction of the tips of both dendrites, so that the solute layer near the tips of both dendrites becomes thinner, and the growth direction of the favorable dendrites is less different from the direction of the temperature gradient, and their growth rate is larger than the tip growth rate of the unfavorable dendrites for an initial period. However, since the orientation angle of unfavorable dendrites is larger than that of favorable dendrites, the effect of convection on the growth of unfavorable dendrites is also greater, so the difference in tip growth rate between unfavorable and favorable dendrites decreases under the continuous influence of convection.

Figure 17 shows the average tip growth rates of the favorably oriented dendrite FO1 and the unfavorably oriented dendrite UO1 for $\Theta_{UO}=-10°$, $\Theta_{UO}=-15°$, and $\Theta_{UO}=-20°$ in configuration 3, as well as the average tip growth rate difference between FO1 and UO1 in the two states. It can be seen from the figure that the average tip velocity difference ΔS_{UO1} of the unfavorable dendrites is greater than the average tip velocity difference ΔS_{FO1} of the favorable dendrites when $\Theta_{UO}=-10°$ and $\Theta_{UO}=-15°$. It indicates that the presence of convection in the grain boundary has a significantly greater effect on the growth rate of unfavorable dendrite tips than on the growth rate of favorable dendrite tips, which is consistent with the pattern presented by conformation 1 and conformation 2. When $\Theta_{UO}=-20°$, the average tip velocity difference for unfavorable dendrites is $\Delta S_{UO1}=0.17$ μm/s and it is $\Delta S_{FO1}=0.12$ μm/s for favorable dendrites. It can be seen that the effect of convection on the growth rate of favorable dendrite tips is more pronounced under this condition. This is because the growth tilt direction of the favorable and unfavorable grains in configuration 3 is the same, and under the influence of convection, the tip growth rate of both dendrites is promoted. When the orientation angle of unfavorable dendrites is larger, the difference in tip height between the favorable and unfavorable dendrites is also larger, and convection can act directly on the tips of the favorable dendrites. By comparing the above three configurations at different angles, there exists a difference of the average tip growth rate between the favorably oriented dendrite FO1 and the unfavorably oriented dendrite UO1. It is found that when $\Theta_{UO}=-10°$, the convection has the greatest effect on the growth of favorable dendrites for configuration 3 and the least effect for configuration 2, while the greatest effect on the growth of unfavorable den-

drites for configuration 1 and the least effect for configuration 3. When $\Theta_{UO} = -15°$, the convection has the greatest effect on the growth of favorable dendrites for configuration 3 and the least effect for configuration 2, while the greatest effect on the growth of unfavorable dendrites for configuration 1 and the least effect for configuration 2. When $\Theta_{UO} = -20°$, the convection has the greatest effect on the growth of favorable dendrites for configuration 3 and the least effect for configuration 1, while the greatest effect on the growth of unfavorable dendrites for configuration 1 and the least effect for configuration 3.

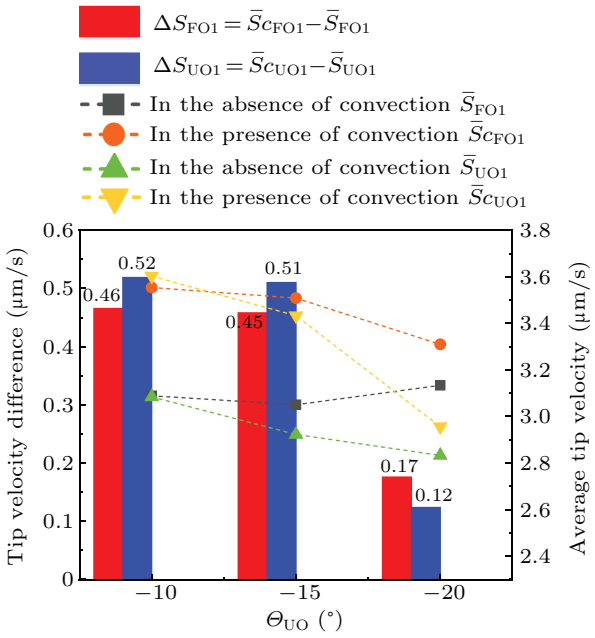


Fig. 17. Average tip growth rates for $\Theta_{UO} = -10°$, $\Theta_{UO} = -15°$, and $\Theta_{UO} = -20°$ in configuration 3 for the favorably oriented dendrite FO1 and the unfavorably oriented dendrite UO1, and the average tip growth rate difference between FO1 and UO1 in the two states.

4. Conclusion

In summary, we have constructed a multi-phase-field-lattice Boltzmann model to simulate the competitive growth process of converging bi-crystals under forced convection conditions. The growth patterns of convergent bi-crystal competition for three configurations are studied separately, and the anomalous elimination behavior of dendrite competition at grain boundaries is analyzed. The results of the present study further extend the elimination mechanism of converging bi-crystals under convective conditions during the evolution of competitive growth. All computational simulations in this study are carried out using the GPU-CUDA parallel computing methods. The conclusions are as follows.

(i) Under pure diffusion conditions, the elimination mechanism of converging bi-crystal competition for all three configurations follows the Walton–Chalmers theory (favorable dendrites eliminate unfavorable dendrites). However, when forced convection is introduced at the grain boundaries, the elimination mechanism of dendrite competition changes under some conditions (anomalous elimination in which unfavorable dendrites eliminate favorable dendrites). This phenomenon is stronger in the converging bi-crystals of conformation 1 and conformation 2 and relatively weaker in conformation 3. Specifically, under the influence of convection, when $\Theta_{UO} = -10°$, conformation 1 and conformation 2 undergo anomalous elimination during the competitive growth of converging bi-crystals, while conformation 3, though showing a tendency to undergo anomalous elimination, does not eliminate the favorable dendrites during the evolutionary time.

(ii) When convection is introduced in the liquid phase, the growth rates of all dendrites in the grain boundary are affected, and the tip growth rates of favorable and unfavorable dendrites in different configurations are affected to different degrees. By further comprehensive comparison of the dendrite tip growth rates of different configurations, it is found that when $\Theta_{UO} = -10°$, the forced convection has the greatest effect on the growth of the favorable dendrite for configuration 3 and the least effect for configuration 2, while the greatest effect on the growth of the unfavorable dendrite is for configuration 1 and the least effect for configuration 3. When $\Theta_{UO} = -15°$, the convection has the greatest effect on the growth of favorable dendrites for configuration 3 and the least effect for configuration 2, while the greatest effect on the growth of unfavorable dendrites for configuration 1 and the least effect for configuration 2. When $\Theta_{UO} = -20°$, the convection has the greatest effect on the growth of favorable dendrites for configuration 3 and the least effect for configuration 1, while the greatest effect on the growth of unfavorable dendrites for configuration 1 and the least effect for configuration 3. The presence of convection in the grain boundary certainly has a positive effect on the growth rate of most converging bi-crystals.

(iii) The solution of the model is designed on the GPU platform regarding the CUDA parallel technique, which realizes the parallelization of computing the multi-phase-field-lattice Boltzmann model in the two-dimensional case and effectively improves the computational efficiency. A comprehensive comparison of the speedup ratios obtained by serial and parallel computing methods shows that GPU-based parallel computing of the model has an absolute advantage, and the parallel speedup becomes more obvious as the computational area increases. At a computation area of 1500×1500, the speedup ratio is approximately 22.5 times that of the serial computation.

Acknowledgements

Project supported by the National Natural Science Foundation of China (Grant Nos. 52161002, 51661020, and 11364024), the Postdoctoral Science Foundation of China (Grant No. 2014M560371), and the Funds for Distinguished

Young Scientists of Lanzhou University of Technology, China (Grant No. J201304).

References

[1] Deng P R and Li J G 2006 *Rare Metal Mater. Eng.* **35** 1311 (in Chinese)
[2] Trempa M, Reimann C, Friedrich J, Müller G and Oriwol D 2012 *J. Crystal Growth* **351** 131
[3] Walton D and Chalmers B 1959 *J. Heat Transf.-Trans. ASME* **215** 447
[4] Rappaz M and Gandin Ch A 1993 *Acta Metall. Mater.* **41** 345
[5] Rappaz M, Gandin Ch A, Desbiolles J L and Thevoz Ph 1996 *Metall. Mater. Trans. A* **27** 695
[6] D'souza N, Ardakani M G, Wagner A, Shollock B A and McLean M 2002 *J. Mater. Sci.* **37** 481
[7] Zhou Y Z 2011 *Scr. Mater.* **65** 281
[8] Meng X B, Lu Q, Zhang X L, Li J G, Chen Z Q, Wang Y H, Zhou Y Z, Jin T, Sun X F and Hu Z Q. 2012 *Acta Mater.* **60** 3965
[9] Li J J, Wang Z J, Wang Y Q and Wang J C 2012 *Acta Mater.* **60** 1478
[10] Asta M, Beckermann C, Karma A, Kurz W, Napolitano R, Plapp M, Purdy G, Rappaz M and Trivedi R 2009 *Acta Mater.* **57** 941
[11] Zhu C S, Gao Z H, Lei P, Feng L and Zhao B R 2022 *Chin. Phys. B* **31** 068102
[12] Xing H, Ji M, Dong X, Wang Y, Zhang L and Li S 2020 *Mater. Design* **185** 108250
[13] Guo C W, Li J J, Wang Z J and Wang J C 2018 *Mater. Design* **151** 141
[14] Laxmipathy V P, Wang F, Selzer M and Nestler B 2021 *Comput. Mater. Sci.* **186** 109964
[15] Takaki T, Sakane S, Ohno M, Shibuta Y and Aoki T 2020 *Comput. Mater. Sci.* **171** 109209
[16] Sun W Z, Yan R, Zhang Y Z, Dong H B and Jing T 2019 *Comput. Mater. Sci.* **160** 149
[17] Song Y, Akamatsu S, Bottin-Rousseau S and Karma A 2018 *Phys. Rev. Mater.* **2** 053403
[18] Ofori-Opoku N and Provatas N 2010 *Acta Mater.* **58** 2155
[19] Karma A and Rappel W J 1998 *Phys. Rev. E* **57** 4323
[20] Echebarria B, Karma A and Gurevich S 2010 *Phys. Rev. E* **81** 021608
[21] Chen S and Doolen G D 1998 *Ann. Rev. Fluid Mech.* **30** 329